photonics

MDPI

Article

Stimulated Emission in Vertically Aligned Hexagonal ZnO Microcrystals Synthesized by Magnetron Sputtering Method

Andrey P. Tarasov *, Arsen E. Muslimov and Vladimir M. Kanevsky

Shubnikov Institute of Crystallography, Federal Scientific Research Centre "Crystallography and Photonics" of Russian Academy of Sciences, 119333 Moscow, Russia
* Correspondence: tarasov.ap@phystech.edu

Abstract: This study is devoted to the luminescence and stimulated emission properties of the ZnO hybrid structure, which is vertically aligned microcrystals with the [0001] crystallographic orientation and a pronounced hexagonal shape formed on a continuous layer of micron thickness. These microcrystals are up to 10 μm high and up to 8 μm in diameter and form the main part of the structure's thickness. The structure was synthesized on the $M(10\bar{1}0)$ plane of sapphire using the magnetron sputtering method. Luminescence of the structure, represented only by conventional near-UV and green components under low-intensity continuous photoexcitation, confirms its high structural and optical quality. Under pulsed photoexcitation with relatively high intensity, stimulated emission (SE) was observed from the structure in the near-UV region at room temperature. The threshold power density for SE was 0.1–0.2 MW/cm^2. Exceeding the threshold leads to a significant increase in the emission intensity compared to the control film without [0001] microcrystals, also grown on $M(10\bar{1}0)$ sapphire. It was assumed that the optical gain is provided by the whispering gallery modes of individual [0001] microcrystals as a result of inelastic exciton–electron scattering, at least at near-threshold excitation intensities.

Keywords: ZnO; stimulated emission; lasing; whispering gallery mode; microrods; film; vertical alignment; magnetron sputtering; exciton–electron scattering; *M*-plane sapphire

Citation: Tarasov, A.P.; Muslimov, A.E.; Kanevsky, V.M. Stimulated Emission in Vertically Aligned Hexagonal ZnO Microcrystals Synthesized by Magnetron Sputtering Method. *Photonics* **2022**, *9*, 871. https://doi.org/10.3390/photonics9110871

Received: 31 October 2022
Accepted: 16 November 2022
Published: 17 November 2022

1. Introduction

Due to the high quantum yield of near-band-edge (NBE) emission, the high optical gain, and the refractive index, ZnO structures are able to demonstrate intense UV luminescence and stimulated emission (SE) [1]. SE and lasing in the near-UV range have been observed in many ZnO micro- and nanostructures upon optical and electrical excitation, including microcrystals [2,3], films [4,5], and nanocrystals of various types, e.g., 1D nanorods and nanowhiskers [6–8] and 2D nanowalls [9,10] at low temperatures and room temperature (RT).

The excitation of stimulated effects usually requires a high crystalline quality of the samples. In particular, speaking of ZnO films, these phenomena are observed at RT most often only in very high-quality thin films up to 1 μm thick [11–14]. Large film thickness hinders SE excitation as a result of the low density of the created electron–hole pairs, large optical losses due to scattering at grain boundaries, and weak resonant conditions. The only exception is perhaps polycrystalline films of different thicknesses with a pronounced disordered structure, in which optical gain is reached as a result of multiple light scattering (random lasing effect) [4,15,16]. It is much easier to excite SE and observe the laser effect in individual ZnO micro- and nanocrystals, which provide a much higher optical quality factor compared to films. The optical modes that are most commonly formed in such nano/microlasers are Fabry–Perot modes (FPMs) and whispering gallery modes (WGMs). At the same time, due to the total internal reflection and, consequently, low optical losses, ZnO microlasers with WGMs usually demonstrate much higher *Q*-factors and lower laser thresholds compared to their FPM counterparts [3,17]. The most popular method for fabricating such crystals is the vapor transport method, which allows one to form arrays of crystallites with high structural and optical quality in relatively short synthesis times [2,7–9,18,19]. On the positive side, other methods, including chemical bath deposition [10,20] and carbothermal synthesis [21–23], have also proven themselves in the creation of ZnO laser crystals and structures. Some attempts have been made to synthesize laser crystals using hydrothermal growth [24,25] and pulsed laser deposition [26]. However, synthesis using these methods often requires solving an additional problem of ordering crystals within an array. Seeds and catalysts are usually used for this [6–9]. Frequently, buffer/seed or catalyst layers are formed by magnetron sputtering for further growth of aligned ZnO crystals by other methods [20,27–29]. There are also reports of using the magnetron sputtering method to grow directly optical ZnO nano- and microcrystals, including those exhibiting a certain orientation in space. For example, in [30], the authors fabricated an array of vertically aligned ZnO nanorods ~ 100 nm in diameter and ~ 1 μm in height. In [31], using seed-assisted magnetron sputtering, ZnO microrods 5–10 μm long and up to 1 μm in diameter were synthesized; however, such microrods were randomly located on the substrate. It is also worth noting that there is a certain difficulty in obtaining UV-emitting ZnO structures, especially laser structures, by the magnetron method due to the abundant formation of defects that reduce the optical quality of the structure and affect the NBE region of the spectrum [12,31,32].

In [33], using the magnetron sputtering method, we managed to obtain a ZnO hybrid film structure with individual vertically aligned [0001] microcrystals on a continuous smooth layer in a single synthesis experiment without changing synthesis parameters. In such a structure, the possibility of SE excitation in the near UV range was revealed. In the present work, we study the luminescence and SE properties of such a ZnO hybrid structure, setting the localization of SE in the structure, the interpretation of its nature, and the determination of the type of optical modes excited as the main tasks.

2. Materials and Methods

$M(10\bar{1}0)$-plane sapphire substrates were used to grow ZnO structures via magnetron sputtering (discharge current, 100 mA) at a temperature of 810 °C in an oxygen atmosphere (pressure, 1.33 Pa). The synthesis time for a hybrid film structure (hereafter, hybrid sample or hybrid structure) was 90 min. According to the growth model proposed in [33], the formation of the [0001] phase during the synthesis occurs at the second stage of growth. For comparison, a second sample, which was a film approximately 1.2 μm thick (hereafter, control sample or control film,) was grown. Its synthesis time was 15 min.

Structural studies of the films were performed via the X-ray diffraction (XRD) method in the Bragg–Brentano geometry using a PANalytical Empyrean diffractometer. Radiation from a copper anode (CuK_{α} = 1.54 Å) was used. XRD patterns were analyzed, and reflection peaks were identified using the ICSD database (PDF-2) and the High Score Plus program. Microscopic studies of the samples were carried out via scanning electron microscopy (SEM) using a Jeol Neoscope 2 (JCM-6000) microscope.

Photoluminescence (PL) of the samples was observed under excitation with the 3rd harmonic (355 nm) of a Q-switched Nd:YAG laser. The pulse duration and the repetition rate were ~10 ns and 15 Hz. The size of an excitation spot on the samples was ~200 μm. Emissions of the samples were registered with the use of a Peltier-cooled charge-coupled device camera placed behind the exit slit of a monochromator. To obtain a better signal-to-noise ratio, we applied the averaging of spectra using pulse accumulations. In addition, PL excitation in a low-density regime was also performed using spectrally selected 315 nm radiation emitted by a xenon lamp built into a Varian Cary Eclipse Fluorescence Spectrometer. The spectra of directional reflectance (at an angle of 25°) of the samples were measured using a Solar PB2201 UV-Vis spectrophotometer.

3. Results

Figure 1 shows SEM images of the hybrid (Figure 1a) and control (Figure 1b) samples. It can be seen that the hybrid sample's surface is characterized by the presence of individual microcrystals up to 10 μm high and up to 8 μm in diameter with a pronounced hexagonal shape on the surface of a continuous layer. Compared to the inhomogeneous morphology of the hybrid sample, the control sample's morphology turns out to be quite homogeneous. It is a film with a periodic submicrorelief of its surface; however, no individual large microcrystals are observed in this case.

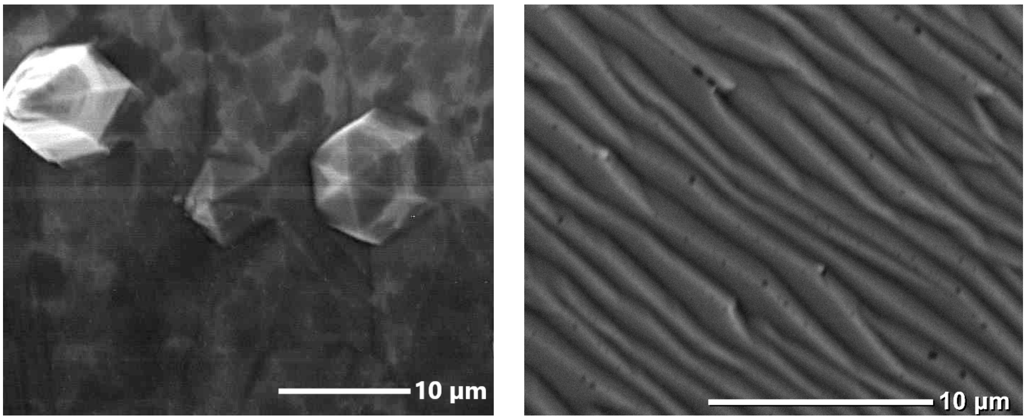

(**a**) (**b**)

Figure 1. SEM images of ZnO samples' surface: (**a**) Hybrid sample; (**b**) control sample.

The results of XRD analysis indicate that both ZnO samples crystallized in the wurtzite structure but are characterized by different preferred orientations (Figure 2). In the XRD pattern of the control film (Figure 2, top), there is only one peak corresponding to the ZnO structure at an angle of 62.8°, which corresponds to the reflection from the (103) plane. The hybrid sample structure is characterized by the main 0002 reflection peak and several much weaker $10\bar{1}1$, $10\bar{1}2$, and $10\bar{1}3$ reflections (Figure 2, bottom).

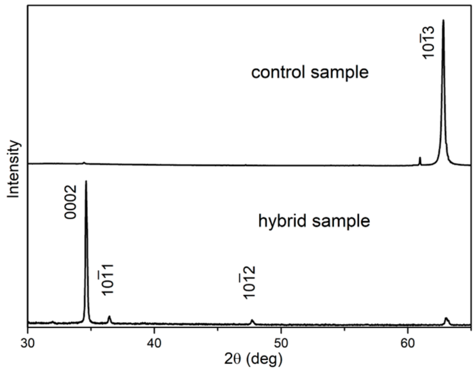

Figure 2. XRD patterns of ZnO structures grown on the *M* plane of sapphire: Hybrid sample (bottom), control sample (top).

During the initial growth of ZnO on the $M(10\bar{1}0)$ plane of sapphire, the following orientation relationship is satisfied: $(10\bar{1}3)_{ZnO} \parallel (10\bar{1}0)_{Al_2O_3}$ [34]. As the target sputtering rate increases, the conditions for the epitaxial nucleation of ZnO on the $M(10\bar{1}0)$ sapphire substrate worsen. Along with epitaxial $[10\bar{1}3]$ nuclei, nuclei of other orientations [0001], $[10\bar{1}1]$, $[10\bar{1}2]$ are formed. Since the (0001) plane in the ZnO structure has the lowest surface energy, as the synthesis continues further, a morphologically inhomogeneous structure with pronounced [0001] ZnO microcrystals is formed. These microcrystals have a hexagonal cross-sectional shape in the plane perpendicular to their *c*-axis, which is, in turn, directed close to the normal to the continuous film surface. Thus, such a hybrid structure is formed in two main stages: (*i*) The formation of the (10$\bar{1}$3) film directly on the substrate and (*ii*) the formation of the (0001) phase, followed by the dominant growth of individual hexagonal microcrystals. These stages are visualized in the diagram presented in Figure 3.

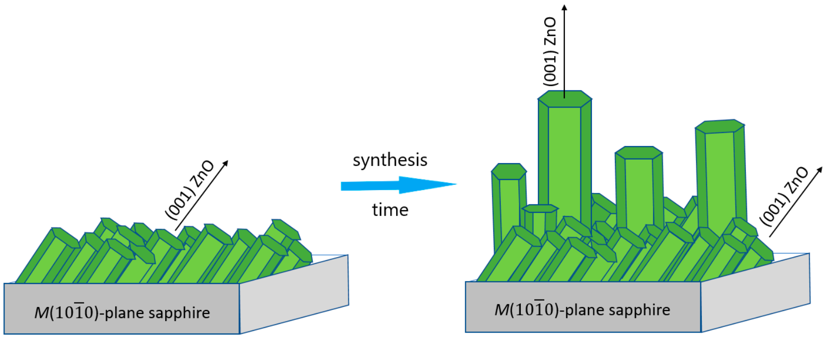

Figure 3. Proposed growth scheme for hybrid ZnO structure.

The directional reflectance spectra of the samples presented in Figure 4a show strong oscillations coming from film interference. In the case of the hybrid sample, this phenomenon apparently occurs in the continuous layer of the structure. Note that the spectral density of the interference fringes is similar for both samples, which suggests nearly the same thickness of the control film and a continuous ZnO layer of the hybrid sample. A simple estimate of the continuous layer thickness from the interference pattern, taking the refractive index dispersion for ZnO, e.g., from [35], yields a value of ~1.5 µm, which corresponds to the known thickness of the control film. Since the heights of the individual [0001] microcrystals formed on the surface of the hybrid structure were different, it is not entirely correct to speak on the certain thickness of the structure. However, SEM data suggest that these microcrystals form the main part of the structure's thickness.

Figure 4b shows the PL spectra in the near UV and visible regions of the hybrid sample recorded at a low-intensity excitation using a Xe lamp (upper spectrum) and under laser excitation with a power density ρ_{exc} = 0.03 MW/cm^2 (lower spectrum). In the first case, the PL spectrum consists of UV and visible components with maxima at 377 nm (3.29 eV) and 505 nm (2.46 eV), respectively. The UV component is known as ZnO NBE emission and in our case is likely to be excitonic in nature given the micron size of the structure [36,37]. This band is partially overlapped with the broad visible component, the full width at half maximum of which is ~120 nm (0.6 eV). Visible luminescence is often referred to as the deep-level emission (DLE) of ZnO. DLE peaking in the green part of the spectrum is associated with radiative transitions involving the energy levels of intrinsic defects, particularly oxygen vacancies [1,35].

Upon pulsed laser excitation with the lowest energy used (Figure 4b, bottom), the sample exhibits only ZnO NBE emission with a maximum of 379 nm (~3.27 eV). The strong difference from the case of *cw* low-intensity excitation, where the contribution of DLE to the spectrum is much stronger, can be due to at least two reasons: Saturation of DLE centers [38] and a decrease in the thickness of the depletion layer as a result of band flattening [39].

The evolution of NBE emission of the hybrid structure with increasing ρ_{exc}, shown in Figure 4c, demonstrates a significant transformation of the spectrum shape. At initial excitation intensities, a single band is visually observed in the PL spectrum with a maximum in the region of 379 nm. With an increase in ρ_{exc}, starting from ρ_{exc} ~0.1 MW/cm^2, in the region of ~391 nm (3.17 eV), a second, longer-wavelength band appears and begins to grow rapidly. As ρ_{exc} increases further, this band grows much faster than the short-wavelength component, shifting first to the short-wavelength side (up to 389 nm) due to mutual amplification of the bands, and then to the long-wavelength side. For ρ_{exc} values above 0.13 MW/cm^2, the PL intensity in the region of the long-wavelength band begins to predominate, and the spectrum maximum begins to be determined by the long-wavelength component. In this context, it is useful to compare the obtained results for NBE emission with the case of the control sample, which has a more homogeneous surface morphology. Figure 4d shows the evolution of the NBE emission spectra of the control film with increasing ρ_{exc}. In this case, two spectral bands are not observed: The PL spectrum is represented by only one asymmetric band, the maximum of which is at 379 nm at the lowest excitation intensity, i.e., in the same spectral region as the maximum of the short-wavelength band of the hybrid sample.

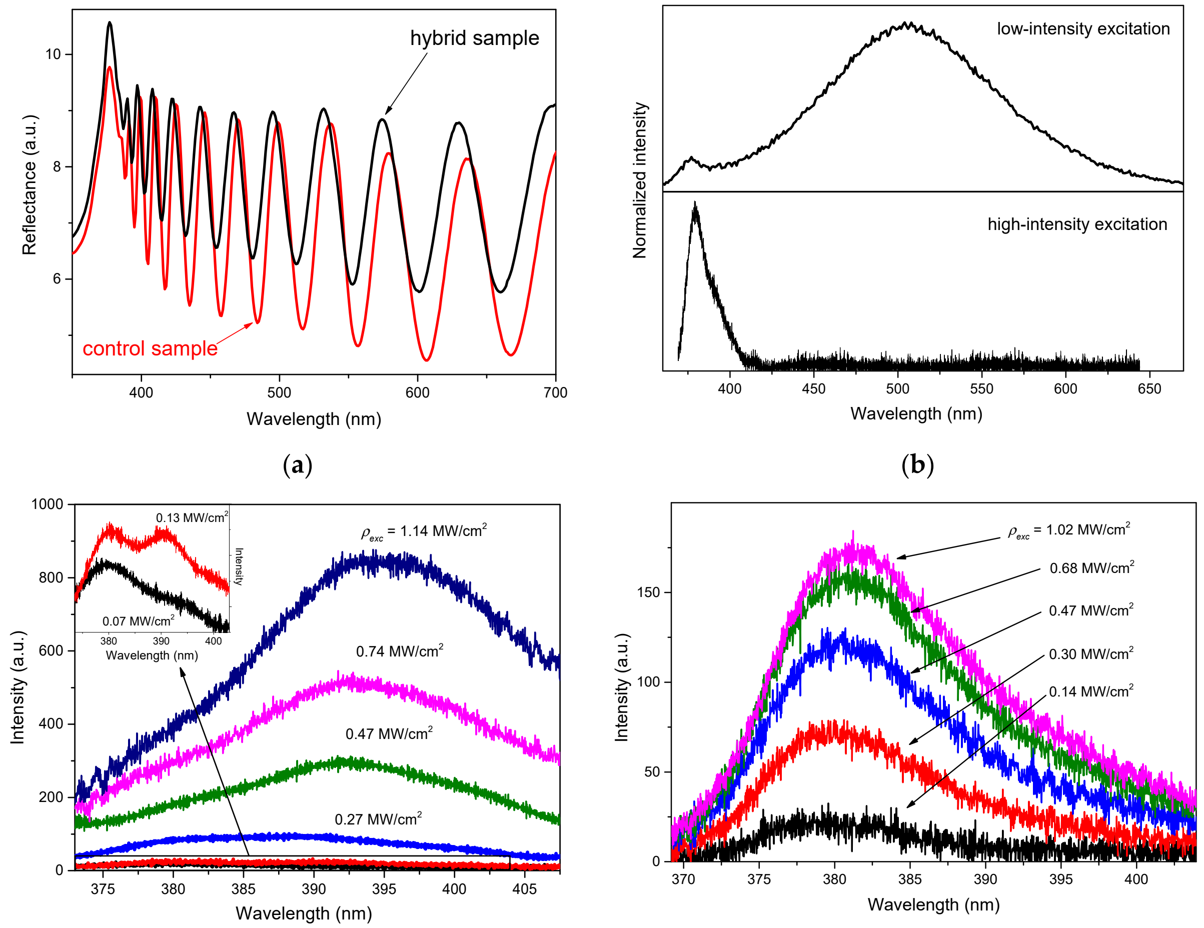

(**a**) (**b**)

(**c**) (d)

Figure 4. Optical and emission properties of the samples: (**a**) Directional reflectance spectra for the hybrid (black) and control (red) samples; (**b**) PL spectra of the hybrid sample at *cw* low-intensity (top) and pulsed high-intensity (bottom) excitations; (**c**,**d**) NBE emission spectra of the hybrid (**c**) and control (**d**) samples at different excitation power densities ρ_{exc}.

Figure 5a plots the dependence of the integral intensity I_{int} of the NBE emission (integration range from 370 to 440 nm) on ρ_{exc} for the hybrid (Figure 5a, black line) and control (Figure 5a, red line) samples. It can be seen that at the initial levels of photoexcitation, both dependences $I_{int}(\rho_{exc})$ are linear with approximately the same slope. For the control sample, this linear dependence can be traced up to 0.6–0.7 MW/cm^2, after which the NBE emission intensity saturates. At the same time, $I_{int}(\rho_{exc})$ in the case of the hybrid sample exhibits bending at ρ_{exc} ~0.18 MW/cm^2, i.e., in the region of a sharp rise of the long-wavelength component compared to the short-wavelength one. With a further increase in ρ_{exc}, the slope of the $I_{int}(\rho_{exc})$ dependence sharply increases (by a factor of ~4.4). Thus, the linear behavior of $I_{int}(\rho_{exc})$ in its initial section for the hybrid sample and in a wider ρ_{exc} range for the control sample indicates the spontaneous nature of the emission. At the same time, the presence of the bending of the $I_{int}(\rho_{exc})$ dependence in the case of the hybrid sample indicates the appearance of SE with a threshold in the bending region in the sample's structure and likely even the onset of lasing. The inset in Figure 5a shows the dependences of the full width at half maximum (FWHM) of NBE emission of the samples on the ρ_{exc}. While in the case of the control film FWHM shows a smooth change over the entire range of ρ_{exc}, the dependence of FWHM on ρ_{exc} for the hybrid structure is slightly more complex. In particular, a sharp rise in FWHM with an initial increase in ρ_{exc} is associated with the appearance of a long-wavelength band in the PL spectrum of the hybrid structure. The subsequent decrease in FWHM in the region of ρ_{exc} ~0.3 MW/cm^2 can be explained by the stimulated character of this band. Due to the contribution of the widths of both short- and long-wavelength bands to the FWHM value, an intense redshift of the long-wavelength band leads to a smooth increase in the FWHM with a further increase in ρ_{exc}. At ρ_{exc} above 0.7–0.8 MW/cm^2, the contribution of the short-wavelength spontaneous emission band to FWHM becomes increasingly insignificant, which results in the FWHM decrease.

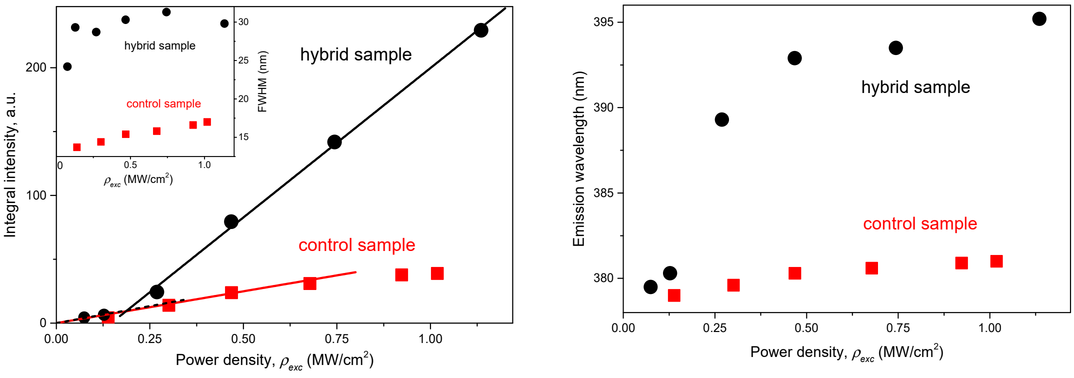

(**a**) (**b**)

Figure 5. Dependences of the integral intensity (**a**) and wavelength in maximum (**b**) of NBE emission for the hybrid (black) and control (red) samples on ρ_{exc}. Lines represent linear fitting; in the case of the hybrid sample, there are two linear parts—before (dashed line) and after (solid line) the SE threshold. The inset in (**a**) shows FWHM of the emission peaks of the samples vs. ρ_{exc}.

Figure 5b compares the dependences of the NBE emission wavelength (at maximum intensity) for both samples. It can be seen that in both cases, NBE emission exhibits a redshift as ρ_{exc} increases. However, for the hybrid sample, it is much larger. In this case, the shift is provided mainly by the long-wavelength component of the spectrum. Its redshift is ~4.2 nm when ρ_{exc} changes from 0.13 to 1.14 MW/cm^2. In the case of the control sample, the redshift of a single band is ~2 nm in approximately the same range of ρ_{exc}, i.e., more than 2 times less than for the long-wavelength NBE emission band of the hybrid sample.

4. Discussion

Since [0001] microcrystallites in the hybrid structure were formed at the last stage of growth, the reduction in the growth time made it possible to avoid their formation in the control sample. At the same time, a comparison of the ZnO NBE emission spectra of both samples made it possible to reveal significant differences in the shape and behavior of the spectra with a change in the photoexcitation intensity. In particular, a linear response to excitation for the control ZnO film and the conventional shape of its NBE emission spectrum with a single spectral band that does not redshift significantly with increasing photoexcitation intensity indicate the spontaneous nature of the emission in the film. On the other hand, the two-band shape of the NBE emission spectrum of the hybrid sample, its threshold nature, and the rapid redshift of the long-wavelength band with increasing photoexcitation intensity confirm the appearance of SE in the ZnO structure. Moreover, such PL spectra with two bands in the NBE region, demonstrating stimulated characteristics, were not observed under similar excitation conditions in other ZnO films grown on different sapphire planes, including $R(1\bar{1}02)$, $A(11\bar{2}0)$, and $C(0001)$ planes [33]. At the same time, the hybrid structure differs from all other cases, including the morphologically homogeneous control film grown on $M(10\bar{1}0)$-sapphire, by the presence of individual *c*-oriented microcrystals on the surface of the continuous layer. Such microcrystals are well oriented in space so that their *c*-axis is close to normal to the surface of the underlying continuous layer. In addition, they are characterized by rather large sizes and a hexagonal cross-section in the (0001) plane.

The rather large micron thickness of the control film, as well as of other films grown on various sapphire substrates [33], and the strong light scattering in some of them, confirmed by their low directional transmission (see Figures 5 and 6 in [33]), do not allow excitation of stimulated effects in their structure. In this sense, it is unlikely that a continuous layer of the hybrid sample, also having a micron thickness, is an exception. In view of this, we assume that SE in the hybrid sample under the interband excitation used appears in individual vertically aligned [0001] microcrystals. Taking into account the characteristic hexagonal shape of these microcrystals, it can be assumed that the optical gain in them is provided by the whispering gallery modes (WGMs) mainly near the bottom of the visible parts of the crystals, close to the normal to the *c* axis. Similar spectral characteristics of the gain contour, particularly an intense redshift with increasing photoexcitation intensity in the spectral region of 390–395 nm (3.14–3.18 eV), are often demonstrated by ZnO structures with WGMs [2,3,19,40]. Frequently, an inversion in electron–hole plasma (EHP) is claimed to be responsible for the optical gain in the case of such a redshifting band [2,3,19].

As is known, depending on the density of electron–hole pairs n_p, which, in turn, is determined by the photoexcitation intensity, radiative interband recombination followed by NBE emission in ZnO microstructures at RT can occur either in the excitonic or EHP regimes, unless the structure is in the transition state between these regimes [1–3]. A common way to estimate n_p is using the expression $n_p = \rho_{exc}\tau_p(\hbar\omega_{exc}l)^{-1}$ ($\hbar\omega_{exc}$ is the excitation photon energy, τ_p is an electron–hole pair lifetime, and l is the absorption depth or the diffusion length of electron–hole pairs) or similar [41]. Such an estimate does not depend on the features of a particular physical model and is often very useful; however, it is indicative only in extreme cases of low or high excitation intensity (low or high n_p values, respectively), when, with some degree of confidence, one can speak of underachieving or significantly exceeding the threshold Mott density n_M, which is within the range of 5×10^{17}–4×10^{19} cm^{-3} for ZnO, according to various published data [41–43]. At intermediate excitation intensities, it is often difficult to understand which of the regimes is realized in a particular case due to the individual characteristics of the material and the spread of the theoretical values of n_M. In such cases, one can rely on the spectral features observed in the experiment and physical models, for example. In our case, when using τ_p~100 ps and the absorption depth of l~100 nm [42], the estimate gives n_p~10^{18} cm in the threshold region of appearance of the long-wavelength component in the NBE emission spectrum of the hybrid structure. This value is close to the lower boundary of the range for n_M. Underestimation of the efficiency of creating an electron–hole pair upon absorption of an excitation photon and the diffusion length of electron–hole pairs in a crystal classifies this estimation in the upper range.

In [33], regarding a superlinear rise of the $I_{int}(\rho_{exc})$ dependence for the *c*-oriented ZnO film grown on *A*-plane sapphire, the blue shift and narrowing of its NBE emission band were observed at ρ_{exc} above ~0.65 MW/cm^2. We ascribed these effects to the onset of the EHP inversion and the appearance of SE. At a lower ρ_{exc} value, one can likely expect the participation of excitonic processes in luminescence. One can more reliably exclude the possible assumption of the participation of an inverted EHP in the observed SE band of the hybrid structure, at least at relatively low excitation intensities, applying, for example, calculations using the methods of the many-body theory [43]. If we assume that the NBE emission band of the hybrid sample in the case of *cw* excitation is associated mainly with the recombination emission of free excitons, then its wavelength (~377 nm) corresponds to a band gap energy of ~3.35 eV (taking into account an exciton binding energy in ZnO of 60 meV), which is close to the case of bulk ZnO crystals (3.37 eV) [36]. Taking into account that a significant contribution to spontaneous NBE emission in ZnO is often made by phonon replica of free exciton emission, especially in microcrystalline structures [36,37], the estimated value of the band gap energy may be higher. In this case, given the results of [40], where the dynamic change in the band gap energy due to renormalization was estimated in the case of large ZnO microcrystals, the relationship of such a shifting SE band with recombination radiation in an inverted EHP is unlikely since such radiation should be observed in the region of more short waves. All of this allows us to assume that excitons do participate in the SE of the hybrid sample, at least near its threshold. In particular, under the excitation intensities lower and near the SE threshold, a single NBE emission band of the control film and the short-wavelength spontaneous emission band in the PL spectra of the hybrid structure can be associated with free exciton emission and its phonon replicas. At large ρ_{exc}, the transition to the EHP regime is likely.

Several excitonic mechanisms that can lead to an optical gain in ZnO under intermediate-density excitation at RT, particularly in the spectral region of the SE band observed in this work, are reported in the literature. Among such processes, the most likely ones are exciton–exciton (*X*-*X*) [11,16,18] and exciton–electron (*X*-*el*) scattering [13,40,44,45], which cause radiative recombination of a free exciton after inelastic scattering by another exciton and a free electron, respectively, and two-phonon-assisted exciton recombination (*X*-2LO) [14,46].

Usually, based on low-temperature measurements, it is assumed that the emission band associated with the *X*-*X* process (the so-called *P* band) does not experience a strong shift with increasing excitation intensity at RT [11,16,18]. However, a possible shift is sometimes ascribed to an increase in temperature as a result of heating [47]. At the same time, some doubts regarding the possibility of this process in ZnO at RT exist because of the significant damping of the exciton state [41]. However, to be the *P* band, the long-wavelength band in the PL spectra of the hybrid sample is spaced unreasonably far from the NBE emission band observed at *cw* excitation. This spacing is approximately 14 nm (~120 meV) at the appearance of the long-wavelength band, which is greater than the maximum possible distance (~100 meV) between free exciton emission and the *P* band. Thus, we exclude this process in our case. In the case of the *X*-2LO band at RT, no significant redshift with an increasing excitation intensity was found either [14,45]. Meanwhile, the *X*-*e* process often demonstrates a characteristic redshifting nature [13,40,47]. Moreover, in [40], we came to a conclusion regarding the main role of *X*-*el* scattering in the optical gain formed in ZnO isometric microcrystals that support WGM lasing. Taking into account the experimental observations and the estimates made above, we can assume the participation of similar mechanisms in the appearance of SE in the hybrid sample: Optical gain is provided by WGMs in individual hexagonal [0001] ZnO microcrystals as a result of *X*-*el* scattering. When the excitation intensity is much higher than the threshold value, a transition to the EHP state is likely, while the *X*-*el* process can change to the scattering of Coulomb-correlated electron–hole pairs from the EHP by free carriers [40,41].

5. Conclusions

The work is devoted to the study of optical, luminescent, and stimulated emission properties of the ZnO hybrid structure grown by the magnetron sputtering method on $M(10\bar{1}0)$-plane sapphire substrates. The structure consists of vertically aligned microcrystals with a [0001] crystallographic orientation and a pronounced hexagonal shape, formed on a smooth continuous layer of micron thickness. These microcrystals are up to 10 μm high and up to 8 μm in diameter and form the main part of the structure's thickness since the thickness of the continuous layer is approximately a micron.

Stimulated emission was shown to be excited in such a hybrid ZnO structure at thresholds of approximately 0.1–0.2 $\mathrm{MW/cm^2}$. By comparing the results obtained for the hybrid structure, for a morphologically homogeneous $(10\bar{1}3)$ ZnO film also grown on the

M-plane of sapphire, as well as for other ZnO films grown on different sapphire planes from [33], it was shown that the optical gain in the hybrid structure is formed in individual [0001] microcrystals. The hexagonal shape of the microcrystals and the behavior of the stimulated emission spectrum suggested that the main process leading to optical gain is inelastic exciton–electron scattering, at least at relatively low excitation intensities, while the necessary gain is achieved in the whispering gallery modes.

Thus, the work actually demonstrates that using the magnetron sputtering method, it is possible to form vertically aligned ZnO microcavities with whispering gallery modes, which have an optical quality sufficient for stimulated emission excitation. Further research in this direction can be aimed at modifying and optimizing the properties of such a hybrid structure. In particular, it will be useful to achieve control in the formation of laser microcrystals of the required size, shape, and arrangement density.

Author Contributions: Conceptualization, A.P.T.; methodology, A.P.T.; software, A.P.T. and A.E.M.; validation, A.P.T. and A.E.M.; formal analysis, A.P.T.; investigation, A.P.T. and A.E.M.; resources, A.P.T., A.E.M. and V.M.K.; data curation, A.P.T. and A.E.M.; writing—original draft preparation, A.P.T.; writing—review and editing, A.P.T. and A.E.M.; visualization, A.P.T.; supervision, A.P.T., A.E.M. and V.M.K.; project administration, A.P.T., A.E.M. and V.M.K.; funding acquisition, A.P.T., A.E.M. and V.M.K. All authors have read and agreed to the published version of the manuscript.

Funding: This research was performed in the frame of state assignments of the Ministry of Science and Higher Education of the Russian Federation for FSRC "Crystallography and Photonics" RAS and partially funded by the Council of the President of the Russian Federation for State Support of Young Scientists and Leading Scientific Schools (project No. MK-3140.2022.1.2, stimulated emission in ZnO microcrystals).

Institutional Review Board Statement: Not applicable.

Informed Consent Statement: Not applicable.

Data Availability Statement: Not applicable.

Acknowledgments: The authors are grateful to the Kotel'nikov Institute of Radio Engineering and Electronics, Russian Academy of Sciences, particularly laboratory no. 195, for access to experimental equipment (contract for Scientific and Engineering Cooperation on 14 February 2018) and to B.V. Nabatov (FSRC "Crystallography and Photonics") for help in performing *cw* photoluminescence studies.

Conflicts of Interest: The authors declare no conflict of interest.

References

1. Klingshirn, C.F.; Meyer, B.K.; Waag, A.; Hoffmann, A.; Geurts, J. *Zinc Oxide: From Fundamental Properties towards Novel Applications*; Springer: Berlin/Heidelberg, Germany, 2010; 365p.
2. Xu, C.; Dai, J.; Zhu, G.; Zhu, G.; Lin, Y.; Li, J.; Shi, Z. Whispering-gallery mode lasing in ZnO microcavities. *Laser Photon Rev.* **2014**, *8*, 469–494. [CrossRef]
3. Dong, H.; Zhou, B.; Li, J.; Zhan, J.; Zhang, L. Ultraviolet lasing behavior in ZnO optical microcavities. *J. Mater.* **2017**, *3*, 255–266. [CrossRef]
4. Cho, S.; Ma, J.; Kim, Y.; Sun, Y.; Wong, G.K.; Ketterson, J.B. Photoluminescence and ultraviolet lasing of polycrystalline ZnO thin films prepared by the oxidation of the metallic Zn. *Appl. Phys. Lett.* **1999**, *75*, 2761–2763. [CrossRef]
5. Yamamoto, A.; Miyajima, K.; Goto, T.; Ko, H.J.; Yao, T. Biexciton luminescence in high-quality ZnO epitaxial thin films. *J. Appl. Phys.* **2001**, *90*, 4973–4976. [CrossRef]
6. Gargas, D.J.; Toimil-Molares, M.E.; Yang, P. Imaging Single ZnO Vertical Nanowire Laser Cavities Using UV-laser Scanning Confocal Microscopy. *J. Am. Chem. Soc.* **2009**, *131*, 2125–2127. [CrossRef]
7. Vanmaekelbergh, D.; van Vugt, L.K. ZnO nanowire lasers. *Nanoscale* **2011**, *3*, 2783–2800. [CrossRef]
8. Briskina, C.M.; Tarasov, A.P.; Markushev, V.M.; Shiryaev, M.A. Magnetic field influence on the intensity of ZnO random lasing and exciton luminescence. *J. Nanophotonics* **2018**, *12*, 043506. [CrossRef]
9. Tarasov, A.P.; Briskina, C.M.; Markushev, V.M.; Zadorozhnaya, L.A.; Volchkov, I.S. Morphology and random lasing of (110)-oriented ZnO nanowalls. *Opt. Mater.* **2020**, *102*, 109823. [CrossRef]
10. Rosli, N.; Halim, M.M.; Hashim, M.R.; Kamil, W.M.W.A.; Zhuang, G.-Y.; Chan, S.-Y.; Hsu, H.-C. Physical and optical effect of ZnO nanowalls to nanoflakes on random lasing emission. *Results Phys.* **2021**, *27*, 104528. [CrossRef]

11. Bagnall, D.M.; Chen, Y.F.; Zhu, Z.; Yao, T.; Shen, M.Y.; Goto, T. High temperature excitonic stimulated emission from ZnO epitaxial layers. *Appl. Phys. Lett.* **1998**, *73*, 1038. [CrossRef]
12. Gruzintsev, A.N.; Volkov, V.T.; Barthou, C.; Benalloul, P.; Frigerio, J.-M. Stimulated emission from ZnO–SiO2–Si thin film nanoresonators obtained by magnetron sputtering method. *Thin Solid Films* **2004**, *459*, 262–266. [CrossRef]
13. Nakayama, M.; Nakayama, Y. Spatially-Resolved Photoluminescence Study of Temperature Dependence of Exciton Inelastic Scattering Processes in a ZnO Thin Film. *J. Phys. Soc. Jpn.* **2019**, *88*, 083706. [CrossRef]
14. Vasilyev, N.N.; Borisov, E.N.; Novikov, B.V. Exciton-Phonon Stimulated Emission in ZnO Crystalline Film at Room Temperature. *Phys. Solid State* **2020**, *62*, 1774–1779. [CrossRef]
15. Ma, X.; Chen, P.; Li, D.; Zhang, Y.; Yang, D. Electrically pumped ZnO film ultraviolet random lasers on silicon substrate. *Appl. Phys. Lett.* **2007**, *91*, 251109. [CrossRef]
16. Razeen, A.S.; Gadallah, A.-S.; El-Nahass, M.M. Effect of Ag doping on the properties of ZnO thin films for UV stimulated emission. *Phys. B Condens. Matter* **2018**, *538*, 131–137. [CrossRef]
17. Tarasov, A.P.; Briskina, C.M.; Markushev, V.M.; Zadorozhnaya, L.A.; Lavrikov, A.S.; Kanevskii, V.M. Analysis of Laser Action in ZnO Tetrapods Obtained by Carbothermal Synthesis. *JETP* **2019**, *110*, 739–743. [CrossRef]
18. Chen, R.; Ling, B.; Sun, X.W.; Sun, H.D. Room Temperature Excitonic Whispering Gallery Mode Lasing from High-Quality Hexagonal ZnO Microdisks. *Adv. Mater.* **2011**, *23*, 2199–2204. [CrossRef]
19. Dai, J.; Xu, C.; Nakamura, T.; Wang, Y.; Li, J.; Lin, Y. Electron–hole plasma induced band gap renormalization in ZnO microlaser cavities. *Opt. Express* **2014**, *22*, 28831–28837. [CrossRef]
20. Fadzliana, N.; Samsuri, S.A.M.; Chan, S.Y.; Hsu, H.C.; Maryam, W. Influence of Al doping on random lasing in ZnO nanorods. *Opt. Laser Technol.* **2020**, *124*, 106004. [CrossRef]
21. Czekalla, C.; Sturm, C.; Schmidt-Grund, R.; Cao, B.; Lorenz, M.; Grundmann, M. Whispering gallery mode lasing in zinc oxide microwires. *Appl. Phys. Lett.* **2008**, *92*, 241102. [CrossRef]
22. Demyanets, L.N.; Li, L.E.; Lavrikov, A.S.; Nikitin, S.V. Nanocrystalline zinc oxide: Pyrolytic synthesis and spectroscopic characteristics. *Crystallogr. Rep.* **2010**, *55*, 142–148. [CrossRef]
23. Tarasov, A.P.; Lavrikov, A.S.; Zadorozhnaya, L.A.; Kanevsky, V.M. Low-Threshold Whispering-Gallery Mode Lasing in Large-Diameter ZnO Microrods. *J. Exp. Theor. Phys. Lett.* **2022**, *115*, 502–508. [CrossRef]
24. Jang, J.I.; Park, S.; Frazer, N.L.; Ketterson, J.B.; Lee, S.; Roy, B.K.; Cho, J. Strong P-band emission and third harmonic generation from ZnO nanorods. *Solid State Commun.* **2012**, *152*, 1241–1243. [CrossRef]
25. Qin, F.F.; Xu, C.X.; Zhu, Q.X.; Lu, J.F.; Chen, F.; You, D.T.; Zhu, Z.; Manohari, A.G. Optical performance improvement in hydrothermal ZnO/graphene structures for ultraviolet lasing. *J. Mater. Chem. C* **2018**, *6*, 3240–3244. [CrossRef]
26. Okada, T.; Kawashima, K.; Ueda, M. Ultraviolet lasing and field emission characteristics of ZnO nano-rods synthesized by nano-particle-assisted pulsed-laser ablation deposition. *Appl. Phys. A* **2005**, *81*, 907–910. [CrossRef]
27. Li, C.; Fang, G.; Li, J.; Ai, L.; Dong, B.; Zhao, X. Effect of Seed Layer on Structural Properties of ZnO Nanorod Arrays Grown by Vapor-Phase Transport. *J. Phys. Chem. C* **2008**, *112*, 990–995. [CrossRef]
28. Khranovskyy, V.; Lazorenko, V.; Lashkarev, G.; Yakimova, R. Luminescence anisotropy of ZnO microrods. *J. Lumin* **2012**, *132*, 2643–2647. [CrossRef]
29. Appiagyei, A.B.; Han, J.I. Potentiometric Performance of a Highly Flexible-Shaped Trifunctional Sensor Based on ZnO/V_2O_5 Microrods. *Sensors* **2021**, *21*, 2559. [CrossRef]
30. Kang, S.W.; Mohanta, S.K.; Kim, Y.Y.; Cho, H.K. Realization of Vertically Well-Aligned ZnO:Ga Nanorods by Magnetron Sputtering and Their Field Emission Behavior. *Cryst. Growth Des.* **2008**, *8*, 1458–1460. [CrossRef]
31. Rajkumar, P.; Barman, D.; Kashyap, A.; Sarma, B.K. Realization of ZnO microrods and Ag nanoparticles on glass and Si substrates by magnetron sputtering and near band edge photoluminescence enhancement from the exciton-plasmon system. *Mater. Lett.* **2022**, *325*, 132898. [CrossRef]
32. Jazmati, A.K.; Abdallah, B. Optical and Structural Study of ZnO Thin Films Deposited by RF Magnetron Sputtering at Different Thicknesses: A Comparison with Single Crystal. *Mater. Res.* **2018**, *21*, 3. [CrossRef]
33. Muslimov, A.E.; Tarasov, A.P.; Kanevsky, V.M. Interference Phenomena and Stimulated Emission in ZnO Films on Sapphire. *Materials* **2022**, *15*, 6409. [CrossRef] [PubMed]
34. Muslimov, A.E.; Ismailov, A.M.; Grigoriev, Y.V. Epitaxial Growth of Semipolar (103) ZnO Films on the M Plane of Sapphire. *J. Surf. Investig.* **2021**, *15*, 1195–1199. [CrossRef]
35. Morkoc, H.; Ozgur, U. *Zinc Oxide: Fundamentals, Materials and Device Technology*; John Wiley & Sons: New York, NY, USA, 2008; 488p.
36. Wang, L.; Giles, N.C. Temperature dependence of the free-exciton transition energy in zinc oxide by photoluminescence excitation spectroscopy. *J. Appl. Phys.* **2003**, *94*, 973–978. [CrossRef]
37. Rodrigues, J.; Sedrine, N.B.; Correia, M.R.; Monteiro, T. Photoluminescence investigations of ZnO micro/nanostructures. *Mater. Today Chem.* **2020**, *16*, 100243. [CrossRef]
38. Guo, B.; Qiu, Z.R.; Wong, K.S. Intensity dependence and transient dynamics of donor–acceptor pair recombination in ZnO thin films grown on (001) silicon. *Appl. Phys. Lett.* **2003**, *82*, 2290–2292. [CrossRef]
39. Zhang, Z.; Yates, J.T., Jr. Band Bending in Semiconductors: Chemical and Physical Consequences at Surfaces and Interfaces. *Chem. Rev.* **2012**, *112*, 5520–5551. [CrossRef]

40. Tarasov, A.P.; Zadorozhnaya, L.A.; Muslimov, A.E.; Briskina, C.M.; Kanevsky, V.M. Stimulated Emission and Lasing in Polyhedral ZnO Microcrystals. *J. Exp. Theor. Phys. Lett.* **2021**, *114*, 517–523. [CrossRef]
41. Klingshirn, C.; Hauschild, R.; Fallert, J.; Kalt, H. Room-temperature stimulated emission of ZnO: Alternatives to excitonic lasing. *Phys. Rev. B* **2007**, *75*, 115203. [CrossRef]
42. Ozgür, Ü.; Alivov, Y.I.; Liu, C.; Teke, A.; Reshchikov, M.A.; Doğan, S.; Avrutin, V.; Cho, S.-J.; Morkoç, H. A comprehensive review of ZnO materials and devices. *J. Appl. Phys.* **2005**, *98*, 041301. [CrossRef]
43. Versteegh, M.A.; Kuis, T.; Stoof, H.T.C.; Dijkhuis, J.I. Ultrafast screening and carrier dynamics in ZnO: Theory and experiment. *Phys. Rev. B* **2011**, *84*, 035207. [CrossRef]
44. Matsuzaki, R.; Soma, H.; Fukuoka, K.; Kodama, K.; Asahara, A.; Suemoto, T.; Adachi, Y.; Uchino, T. Purely excitonic lasing in ZnO microcrystals: Temperature-induced transition between exciton-exciton and exciton-electron scattering. *Phys. Rev. B* **2017**, *96*, 125306. [CrossRef]
45. Vasilyev, N.; Borisov, E.N.; Novikov, B.V.; Akopyan, I.K.; Labzovskaya, M.E. Random lasing in ZnO self-organized nanoparticles produced by laser induced breakdown. *J. Lumin* **2019**, *215*, 116668. [CrossRef]
46. Michalsky, T.; Wille, M.; Dietrich, C.P.; Röder, R.; Ronning, C.; Schmidt-Grund, R.; Grundmann, M. Phonon-assisted lasing in ZnO microwires at room temperature. *Appl. Phys. Lett.* **2014**, *105*, 211106. [CrossRef]
47. Briskina, C.M.; Markushev, V.M.; Zadorozhnaya, L.A.; Givargizov, M.E.; Kanevsky, V.M. Edge emission of ZnO grown on Si whiskers. *J. Optoelectron. Adv. Mater.* **2021**, *23*, 150–156.